Materials Today Communications 27 (2021) 102246

Contents lists available at ScienceDirect

Materials Today Communications

journal homepage: www.elsevier.com/locate/mtcomm

A first-principles study of the structural, electronic, optical, and vibrational properties for paramagnetic half-Heusler compound TiIrBi by GGA and GGA + mBJ functional

A. Candan [a,*], A.K. Kushwaha [b]

[a] Department of Machinery and Metal Technology, Kırşehir Ahi Evran University, 40100 Kırşehir, Turkey
[b] Department of Physics, K.N. Govt. P.G. College, Gyanpur, Bhadohi, 221304, India

ARTICLE INFO

Keywords:
Density functional theory
Half-Heusler compounds
Bandgap
Optoelectronic properties

ABSTRACT

The structural, electronic, optical, and vibrational properties of half-Heusler compound TiIrBi have been investigated by using the Generalized Gradient Approximation (GGA) and GGA plus modified Becke and Johnson (GGA + mBJ) functional within the Density Functional Theory (DFT). The obtained formation enthalpies and energy-volume curves for the three different atomic arrangements (α, β, and γ) show that γ phase is the most energetically favorable phase. Additionally, among the paramagnetic (PM), ferromagnetic (FM), and antiferromagnetic (AFM) magnetic systems considered for the γ -phase of this compound, the paramagnetic system is found to be the most stable. The spin-polarized electronic band calculations of the TiIrBi compound demonstrate that this material has a semiconductor nature in both the majority and minority spin channels with the direct bandgap of 0.56 and 0.87 eV using the GGA and GGA + mBJ approach, respectively. The obtained formation enthalpy and phonon dispersion curves for γ -crystal structure of TiIrBi compound show that this material is both thermodynamically and dynamically stable. We have also examined the optical properties by computing the optical parameters such as real and imaginary parts of the dielectric function, refractive index, extinction coefficient, optical conductivity, and reflectivity of the half-Heusler compound TiIrBi in the photon energy range of 0–16 eV. The collected results indicate that the TiIrBi compound has a direct bandgap semiconductor, which makes it a convenient material for technological applications in optoelectronics.

1. Introduction

Heusler compounds were firstly discovered in the early 1900s by Friedrich Heusler who a German chemist and mining engineer [1]. He observed that although the elements that make up the Cu_2MnAl compound do not show magnetic properties, it is ferromagnetic at room temperature. Thanks to their extraordinary properties, these materials are used in many areas of device technology. Besides, Heusler compounds are quite stimulating and popular nominees for large-scale technological applications such as solar cells, magneto-optical devices, magnetic tunnel junctions, multi-functional tools, thermoelectrics, and spintronic devices [2–10]. Thus far, there are presently more than 1000 compounds sorted as full-Heusler and half-Heusler whose characteristics can be estimated by calculating the number of their valence electrons. Heusler compounds consist of four interpenetrating face-centered cubic (*fcc*) sublattices and crystallize in the $L2_1$ crystal structure. These compounds in the space group 225 (*Fm-3 m*) are known as full-Heusler compounds expressed by the general formula X_2YZ [11]. In case one of the sublattices is empty, the corresponding material is called a half-Heusler compound. Such compounds crystalize in cubic $C1_b$ crystal structure with space group 216 (*F-43 m*) [12]. The chemical composition of the half-Heusler compound is written as XYZ. Generally, X and Y are transition elements, while Z is the main group element. Half-Heusler compounds with 8 or 18-valence electrons per formula unit usually signify bandgaps subtending to s, p, and d electron shells. The basic physical properties of materials with 8-valence electrons are very similar to conventional semiconductors such as GaAs and Si [13–15]. While semiconductors with 18 valence electrons contain an almost filled d-electron shell, which induces a strong hybridization of the d states of the X and Y elements. It also allows the creation of a closed-shell configuration and a bandgap [16,17]. The compositional modifications permitted by the structure result in adjustable bandgaps in the

* Corresponding author.
E-mail address: acandan@ahievran.edu.tr (A. Candan).

https://doi.org/10.1016/j.mtcomm.2021.102246
Received 2 December 2020; Received in revised form 4 March 2021; Accepted 7 March 2021
Available online 10 March 2021

width of 0–1 eV for the 18-valence electron system, whereas the maximum limit of this gap for all half-Heusler compounds could arrive at 4 eV [18]. As for the 8-valence electron system, the greater electronegativity between the X and Y atoms, the greater the value of the arising bandgap. The bandgap values of half-Heusler systems with 18 valence electrons make them attractive as potential thermoelectric materials [19].

Half-Heusler compounds have attracted considerable interest over the past decade because of their numerous desirable properties such as half-metallic ferromagnets [20], superconductors [21], compensated ferrimagnets [22], shape memory alloys [23], nonmagnetic semiconductors [24], topological insulators [25], and heavy fermion systems [26]. Besides, there are large numbers of investigations regarding these materials in several types of magnetic order, namely, the paramagnetic [27,28], ferromagnetic [29–31], and ferrimagnetic [32].

The Ti, Zr, Hf; Co, Rh, Ir; and As, Sb, Bi atoms successively are part of the IV–IX–V groups, which can be alloyed into countless significant materials with exciting physical features [33,34]. These ternary half-Heusler materials have aroused a great deal of interest within the past decade, and also these compounds have been the subject of many theoretical and experimental investigations in relation to their applications in thermoelectric, optoelectronics, and electronics devices [18, 24,35–43]. Experimentally, Sekimoto et al. [35] have successfully synthesized (Ti, Zr, Hf)CoSb samples employing arc melting technique and also measured the thermoelectric properties of their such as electrical resistivity, thermoelectric power, and thermal conductivity. They emphasized that these alloys have the potential to be an unexplored group of thermoelectric material owing to their great thermoelectric strength and low thermal conductivity. Similarly, Zhao and co-workers [36] synthesized polycrystalline of Pd-doped $ZrCo_{1-x}Pd_xBi$ (x = 0, 0.03, 0.06, 0.09) half-Heusler samples by rapid hot-pressing sintering and arc melting technique. They clearly stated in their study that the Seebeck coefficient and electrical conductivity of the $ZrCo_{1-x}Pd_xBi$ rise owing to the replacement of the Pd with the Co atom. On the theoretical side, phonon and thermoelectric properties of ternary half-Heusler compound HfRhSb have been inspected employing Quantum Espresso package by Kaur et al. [24]. They have reported that HfRhSb has an indirect bandgap of 1.21 eV. With the help of first-principles density functional theory, Ma et al. [37] studied electronic properties and thermoelectric transport properties of the half-Heusler compounds MCoBi (M = Ti, Zr, and Hf). They have shown that these compounds could be a kind of up-and-coming potential nominee for thermoelectric applications. On the other hand, using Heyd-Scuseria-Ernzerhof (HSE) hybrid functional, Gautier et al. [38] estimated over 400 half-Heusler compounds which are devised to be very worthwhile in piezoelectrics, thermoelectrics, and topological insulators. Lately, Dey and co-workers [18] have studied the electronic, structural, optical, and thermoelectric properties of Bismuth-based ZrRhBi, ZrIrBi, and HfRhBi ternary half-Heusler compounds using the full potential linearized augmented plane wave (FP-LAPW) method. The authors pointed out that these three materials have many technological applications as thermoelectric materials in fields such as electronics and optoelectronics.

Aside from these studies, the main physical properties of Bi-based half-Heusler compounds, including HfRhBi, ZrIrBi and ZrRhBi [17], XCoBi (X = Ti, Zr, Hf) [28], ZrXBi (X = Co, Rh) [40], HfRhZ (Z = As, Sb and Bi) [41], HfIrX (X = As, Sb and Bi) [42,43], PtXBi (X = Mn, Fe, Co and Ni) [44], XFeBi (X = Hf and Ti) [45], PtLaBi [46], XX′ Bi (X = Na, K, Rb, Cs; X′ = Ca, Sr) [47], and PrNiBi [48] have been studied using the density functional theory by different groups.

Although many studies on ternary Bi-based half-Heusler compounds have been presented so far, there is no research in the literature concerning the basic physical properties of the TiIrBi compound. In the current investigation, the structural, magnetic, electronic band structure, and optical properties of this compound for three different phases (α, β, and γ) are extensively computed using GGA approximation besides modified Becke–Johnson (GGA + mBJ) potential. The obtained all parameters have been matched with those of other Bi-based half-Heusler compounds to yield a deep understanding of the title compound.

2. Methodology of calculation

The structural, magnetic, electronic, and optical properties of the ternary TiIrBi half-Heusler compound were implemented using the Vienna Ab Initio Simulation Package (VASP) [49,50] with the projector augmented wave scheme (PAW) [51]. Additionally, electron exchange and correlation potentials were also treated within the generalized gradient approximation of Perdew- Burke-Ernzerhof (GGA-PBE) [52] and modified Becke–Johnson (GGA + mBJ) [53–55] potential. The semi-core and valence electrons are in the $3s^2\ 3p^6\ 3d^2\ 4s^2$ configuration for Ti, $5s^2\ 5p^6\ 4f^{14}\ 5d^7\ 6s^2$ configuration for Ir, and $5s^2\ 5p^6\ 4f^{14}\ 5d^{10}\ 6s^2\ 6p^3$ configuration for Bi. The kinetic energy cut-off was 500 eV for the plane-wave basis functions and Monkhorst-Pack type 12 × 12 × 12 k-point [56], which is located at the Γ-point of the zone center and automatically generated, for Brillouin zone integration were taken. However, the 18 × 18 × 18 k-point was used as the examination of optical properties, and electronic band structures which requires more precise calculations. For self-consistent field calculations, the convergence criterion of the total energy and charge was set to 10^{-8} eV and 10^{-7} eV/Å, respectively. Additionally, the smearing technique was applied to the Fermi surface to get a perfectly accurate electronic state density and the smearing parameter was selected as 0.225 eV [57]. The computed crystallographic structure types have been depicted by the VESTA code [58].

3. Results and discussion

3.1. Crystal structure stability of the α, β, and γ phases

The ternary intermetallic compounds, in which X and Y are transition metal atoms and Z are main group atoms are well-known half-Heusler compounds. These compounds crystallize with space group *F-43 m* in MgAgAs-type ($C1_b$) cubic structure. The compounds with structure $C1_b$ are having three interpenetrating face-centered-cubic sub-lattices with rock-salt and zinc-blende structure. In this type of structure, there are three different atomic arrangements with α, β, and γ phases in which the Wyckoff positions of atoms are given in Table 1.

Besides, the crystal structures of the title compound with α, β, and γ phases are also presented in Fig. 1, respectively. The total energy plots as a function of unit cell volume for all structural phases (α, β, and γ) are depicted by fitting to the Murnaghan equation of state [59].

$$E(V) = E_0 + \frac{K_0 V}{K_0^{'}}\left[\left(\frac{V_0}{V}\right)^{K_0^{'}}\frac{1}{K_0^{'}-1}+1\right] - \frac{K_0 V_0}{K_0^{'}-1} \quad (1)$$

where E_0 refers to the ground state energy, K_0 symbolizes the bulk modulus, $K_0^{'}$ represents its first derivative concerning the pressure, and V_0 unit cell volume. As well as the structural stability, structural parameters like lattice constants, bulk modulus, and first derivatives of its, and unit cell volumes have been computed by the fitting process and are summarized in Table 2.

The minimization of total energy procedure is used to know the most stable structural phase among the three phases α, β, and γ of the

Table 1
The Wyckoff position of the atoms for TiIrBi half-Heusler compound with α, β, and γ phases.

Phase	Ti	Ir	Bi
α	(0.5, 0.5, 0.5)	(0, 0, 0)	(0.25, 0.25, 0.25)
β	(0.25, 0.25, 0.25)	(0.5, 0.5, 0.5)	(0, 0, 0)
γ	(0, 0, 0)	(0.25, 0.25, 0.25)	(0.5, 0.5, 0.5)

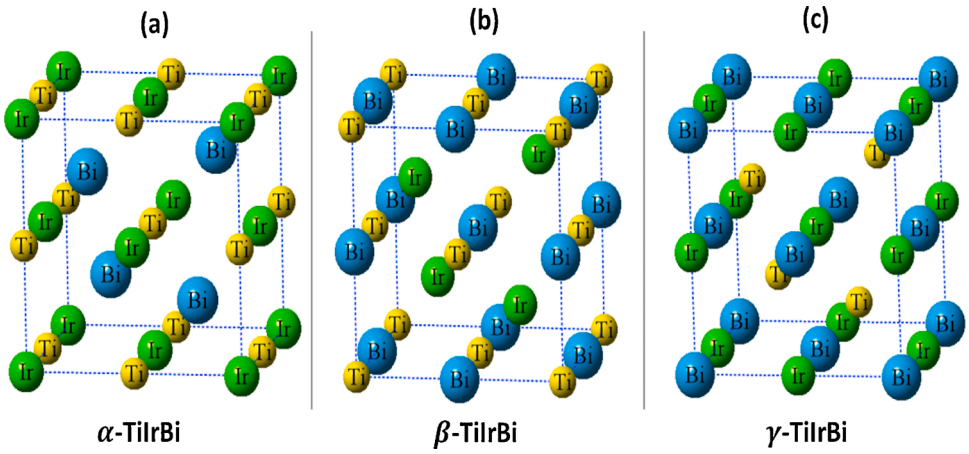

Fig. 1. The crystal structure of TiIrBi half-Heusler compound in (a) α phase, (b) β phase, and (c) γ phase.

Table 2
The calculated structural parameters and formation enthalpies of TiIrBi half-Heusler compound for α, β, and γ phases.

F-43 m	Phase	a_0 (Å)	K_0 (GPa)	$K_0^{'}$	V_0 (Å^3)	ΔH_f (eV/atom)
	α	6.358	106.5	4.54	257.060	0.440
TiIrBi	β	6.324	104.4	4.19	252.955	0.061
	γ	6.309	123.7	4.70	251.139	−0.423

examined compound TiIrBi. Fig. 2 represents that the γ phase of the examined compound is the most stable. The lattice constant, bulk modulus, and derivative of its for γ -TiIrBi half-Heusler compound are obtained as 6.309 Å, 123.7 GPa, and 4.54, respectively. We could find neither experimental nor other theoretical computations about the TiIrBi compound to confirm our results. Therefore, to compare these predicted outcomes for TiIrBi with those of the compounds with similar characteristics, HfIrBi, and ZrIrBi compounds is the nearly most convenient one in that Hf, Zr, and Ti elements have the same number of valence electrons in the outer orbital. In two different studies about ZrIrBi and HfIrBi, the values of the lattice constant (a_0), bulk modulus (K_0), and its pressure derivative ($K_0^{'}$) have been reported 6.410 Å, 150.30 GPa, and 4.84 for ZrIrBi [39]; 6.381 Å, 153.25 GPa, and 4.20 for HfIrBi [42]. The computed lattice constant for γ -TiIrBi deviates from roughly 1.58 % for ZrIrBi, and 1.13 % for HfIrBi, respectively.

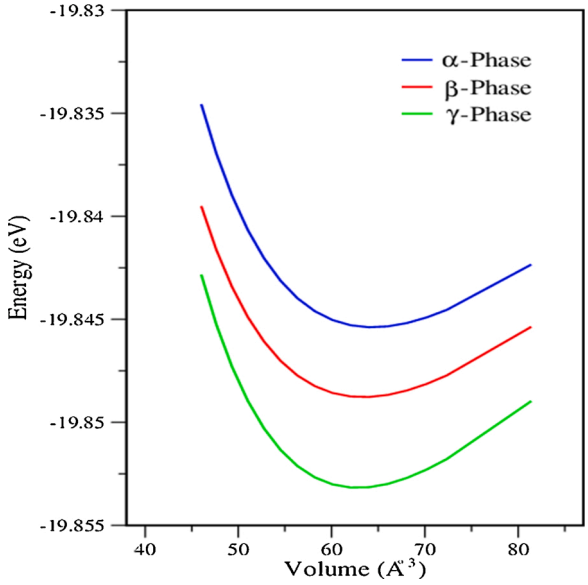

Fig. 2. Total energies as a function of unit cell volume for TiIrBi half-Heusler compound in α, β, and γ phases.

Additionally, to mean the chemical stability of the examined ternary half-Heusler TiIrBi compound, the formation enthalpies ΔH_f (eV/atom) for all phases are obtained and given in Table 2. The computed formation enthalpy values can be used to determine the phase that is most stable in terms of the energy of a crystal in any structural phase [60]. The formation enthalpy is defined as:

$$\Delta H_f = E_{TiIrBi}^{total} - \left[E_{Ti}^{bulk} + E_{Ir}^{bulk} + E_{Bi}^{bulk}\right] \quad (2)$$

where E_{TiIrBi}^{total} is the total energy per formula unit; E_{Ti}^{bulk}, E_{Ir}^{bulk}, and E_{Bi}^{bulk} are the total energy per atom of the pure Ti, Ir, and Bi in their bulk stable states, respectively. As seen in Table 2, α and β phases of the examined compound are having positive formation enthalpy while the γ phase is having negative formation enthalpy. This result suggests that the α and β phases are thermodynamically unstable while the γ phase is thermodynamically stable. It is clear from the calculated formation enthalpy that TiIrBi with γ phase can be synthesized experimentally. There is no other data available in the literature for comparison.

3.2. Magnetic and electronic structure properties

The paramagnetic (PM), ferromagnetic (FM), and antiferromagnetic (AFM) calculations have been done for the TiIrBi compound in the stable γ -phase and the total energy-volume plots are presented in Fig. 3. From Fig. 3, it can be concluded that the most stable magnetic state is PM because of having the minimum ground state energy.

With the intent of studying the electronic nature of the title compound, the spin-polarized electronic band structures along the high symmetry directions have been obtained for both GGA and GGA + mBJ methods and plotted in Fig. 4. The modified Beck-Johnson (mBJ) exchange-correlation potential, which was proposed by Tran and Blaha [54], has been reported to be much more successful than the GGA and LDA approach in estimating bandgaps for large numbers of insulators and semiconductors [61]. It is quite clear for both methods from Fig. 4 that the valence band maximum (VBM) and the conduction band minimum (CBM) arise at the Γ-point verifying a direct bandgap. These direct bandgaps with GGA and GGA-mBJ approximations are 0.56 eV and 0.87 eV, respectively. The plotted band structures of TiIrBi semiconductor for both methods are almost like each other in the energy regions varying from − 6 to 3 eV. One striking point when comparing obtained electronic band structures is that the conduction band shifts towards higher energy and the bandgap is slightly opened within the GGA + mBJ method. As a result, the usage of GGA + mBJ potential in contrast to the GGA approach increases the computed bandgap of TiIrBi

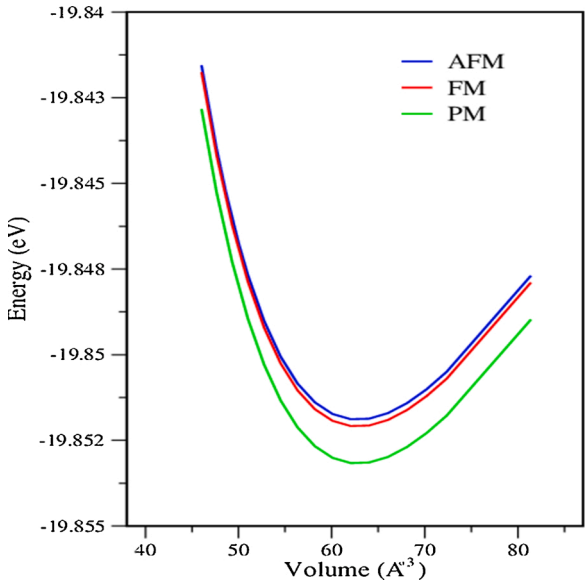

Fig. 3. Total energies as a function of unit cell volume for γ -TiIrBi half-Heusler compound in different magnetic systems.

semiconductor.

To elucidate in more detail the nature of the electronic band structure, the spin-polarized total and partial density of electronic states of the γ -TiIrBi compound are calculated by GGA and GGA + mBJ methods and these are presented in Figs. 5(a–b), and 6 (a–b), respectively. It is obvious in Figs. 5 and 6 that the lower energy band region between -6 eV and -3 eV in the valence band has been constructed by the main contribution of electrons of the *p*-orbitals of Bi-atoms, *s*- and *d*-orbitals of Ir-atoms, and also the main contributions of the electrons of *s*- and *d*-orbitals of Ti-atoms and small contributions of the electrons of the rest of the orbitals. The upper valence region from - 3 eV to 0 eV is formed by the fundamental contribution of *d*-orbitals of Ti- and Ir-atoms, *p*-orbitals of Bi-atoms for both methods. Besides, as can be seen from Fig. 5, there are strong *d-d* hybridizations between *d*-orbitals of Ti-atoms and *d*-orbitals of Ir atoms in this energy range for both GGA and GGA + mBJ. On the other hand, almost no contribution from Bi atoms is realized in the conduction energy region. Therefore, the total density of electronic states in the conduction energy region is mostly owing to the *d*-orbitals of Ti and Ir atoms. Here, we observe a similar partial density of electronic states for GGA (Fig. 5) and GGA + mBJ (Fig. 6). Furthermore, the conduction energy band region is exactly composed of the *d*-orbitals (*d*-e_g, and *d*-t_{2g}) of Ti and Ir atoms for both these methods. Given the foregoing debate, it can be deduced that *d*-electrons of Ti and Ir atoms have an important role in thermoelectric properties.

To clarify the interaction of atoms, the electronic charge density distributions of the investigated compound are drawn using the VESTA program [58]. The two-dimensional (*2-D*) electron charge density plot of the TiIrBi compound on the plane (111) is presented in Fig. 7. The isoelectronic surfaces around all the atoms are spherical in structure, where the bonds between these atoms are elucidated by the ionic bonding nature. It was also reported similar characteristics for other half-Heusler compounds in Refs. [39,62].

3.3. Optical properties

To explain the basic knowledge of optical properties is very important for semiconductor materials, and thereby the relationship between the electronic band structure of a solid crystal and optical properties can be determined [63]. For this reason, the optical properties of semiconductor TiIrBi including real and imaginary parts of the dielectric function as a function of photon energy have been computed with GGA + mBJ in the range of 0−16 eV and presented in Fig. 8(a). The frequency-dependent dielectric function can be written as below [64]:

$$\varepsilon(\omega) = \varepsilon_1(\omega) + i\varepsilon_2(\omega) \tag{3}$$

where $\varepsilon_1(\omega)$ and $\varepsilon_2(\omega)$ are the real and imaginary parts of the dielectric function, respectively. The real part of the dielectric function describes a material's ability to interact with an electric field (store and remit energy) without absorbing energy, whereas the imaginary part of the dielectric function characterizes a material's ability to permanently absorb energy from a time-varying electric field. The imaginary part of the dielectric function is derived from the electronic band structure computations with the help of the following relation [65]:

$$\varepsilon_2(\omega) = \left(\frac{4\pi^2 e^2}{m^2\omega^2}\right)\sum_{ij}\int \langle i|M|j\rangle^2 f_i(1-f_i)\delta(E_j - E_i - \omega)d^3k \tag{4}$$

where e, m, ω and M represent the electron charge, electron mass, photon frequency, and dipole matrix, respectively. E_i is the electron energy of the initial state, E_j is the electron energy of the final state, and f_i is the Fermi occupation factor of the single-particle state *i*.

The real part $\varepsilon_1(\omega)$ of the dielectric function is obtained from the imaginary part taking advantage of the Kramers-Kronig transformations [66,67],

$$\varepsilon_1(\omega) = 1 + \frac{2}{\pi}P\int_0^{\infty}\frac{\omega'\varepsilon_2(\omega')}{\omega'^2 - \omega^2}\,d\omega' \tag{5}$$

where P is the Cauchy principal value. As illustrated in Fig. 8(a), the static dielectric constant of semiconductor TiIrBi at zero frequency ($\omega = 0$) has been computed as $\varepsilon_1(0) = 20.87$ using the GGA + mBJ method. As seen from Fig. 8(a), the real part of dielectric function rises with the rise in photon energy, subsequently; it reaches a maximal value at a photon energy of 1.76 eV ($\varepsilon_1(\omega) = 30.365$) by showing normal distribution character. It starts rapidly to decline by displaying anomalous distribution characters in the range from 1.76 eV to 3.96 eV. On the other side of 4.2 eV photon energy, it goes below zero, and then it approaches zero value at higher energy values.

Electronic properties of a crystal are mainly elucidated by utilizing imaginary part $\varepsilon_2(\omega)$ of the dielectric function which is associated with the event of the absorption of photons. The obtained spectra of $\varepsilon_2(\omega)$ for TiIrBi compound are plotted in Fig. 8(a). The computed threshold value of $\varepsilon_2(\omega)$ with GGA + mBJ approximation is practically 0.86 eV for TiIrBi semiconductor. The source of this point is by dint of the inter-band electronic transition ($\Gamma_c - \Gamma_v$) between the highest valence band and the lowest conduction band at the Γ-point for TiIrBi, and also it is called the fundamental absorption limit. Maximal value of $\varepsilon_2(\omega)$ takes place at approximately 2.20 eV for the TiIrBi compound. Thereafter, a descent in the spectra of this compound can be observed with ascending energy. The obtained optical bandgap value from $\varepsilon_2(\omega)$ is 0.86 eV for TiIrBi, which is in good agreement with the predicted bandgap from electronic band structure calculations (0.87 eV). Besides, the highest peak values in the spectra of $\varepsilon_2(\omega)$ occur in the visible and ultraviolet regions of the electromagnetic spectrum. It can be concluded that the investigated compound is a substantial nominee for optoelectronic devices.

Afterward, other optical parameters like the refractive index $n(\omega)$, extinction coefficient $k(\omega)$, reflectivity $R(\omega)$, and optical conductivity $\sigma(\omega)$ can be obtained from the calculated values of the real and imaginary parts of the dielectric function [42,68].

$$n(\omega) = \left[\frac{\sqrt{\varepsilon_1^2(\omega) + \varepsilon_2^2(\omega)} + \varepsilon_1(\omega)}{2}\right]^{1/2} \tag{6}$$

$$k(\omega) = \left[\frac{\sqrt{\varepsilon_1^2(\omega) + \varepsilon_2^2(\omega)} - \varepsilon_1(\omega)}{2}\right]^{1/2} \tag{7}$$

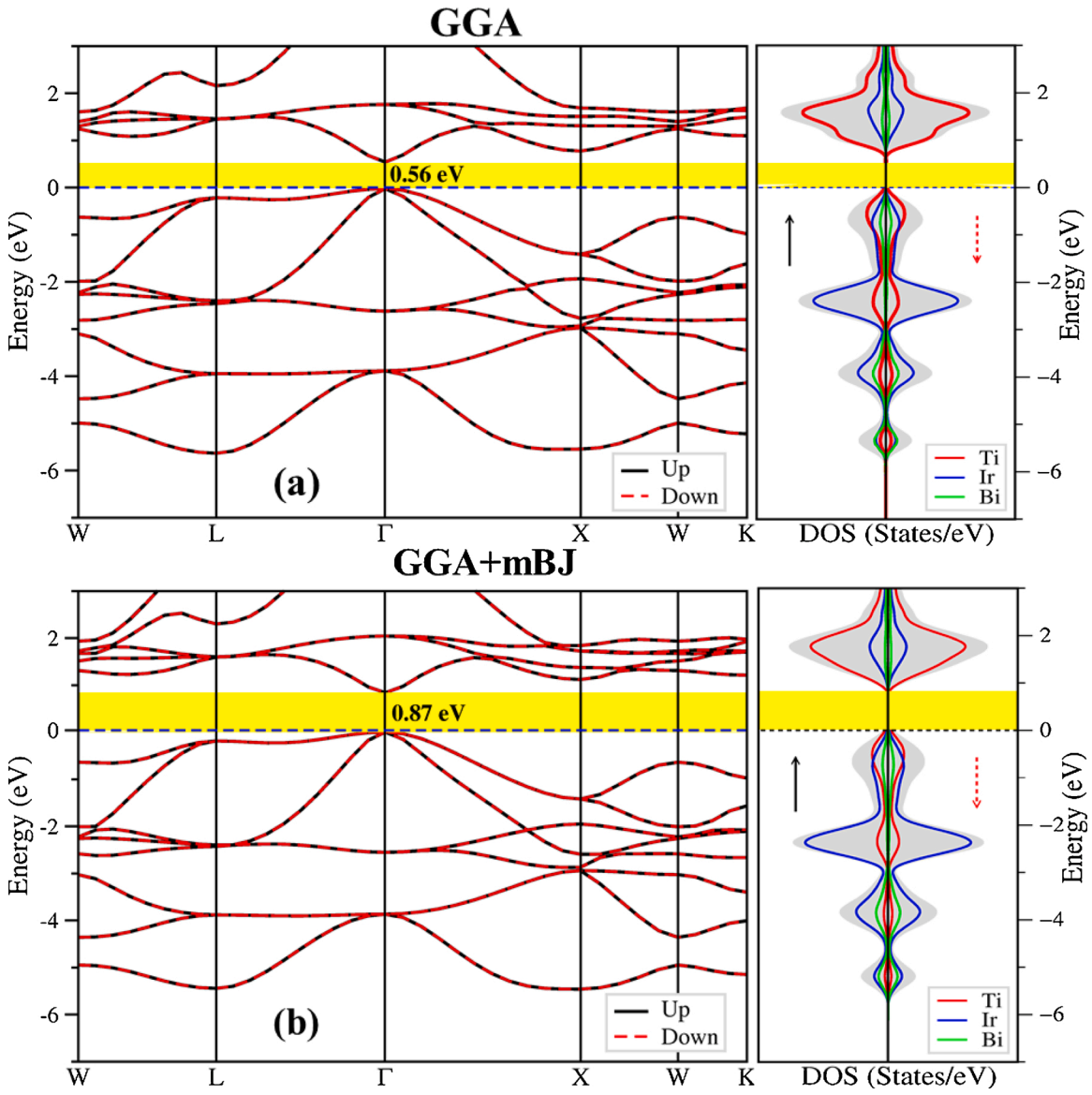

Fig. 4. The spin polarized band structures, total and partial densities of states for γ -TiIrBi half-Heusler compound with (a) GGA, (b) GGA + mBJ. The dashed horizontal lines at zero energy indicate Fermi level.

$$R(\omega) = \left| \frac{\sqrt{\varepsilon(\omega)} - 1}{\sqrt{\varepsilon(\omega)} + 1} \right|^2 \tag{8}$$

$$\sigma(\omega) = -\frac{i\omega}{4\pi} \varepsilon(\omega) \tag{9}$$

Refractive index $n(\omega)$ and extinction coefficient $k(\omega)$ are significant constants to comprehend microscopic interactions with light. The calculated refractive index $n(\omega)$ spectrum for the TiIrBi compound is plotted in Fig. 8(b), having a parallel form with the $\varepsilon_1(\omega)$ spectrum. The value of the refractive index at zero frequency ($\omega = 0$) boundary is defined as a static constant of refractive index $n(0)$ of semiconductor TiIrBi compound. This constant is found as 4.57 for the studied compound. This result shows that the static value of refractive index $n(0)$ is strongly associated with the $\varepsilon_1(0)$ by the following correlation [69],

$$n(0) = \sqrt{\varepsilon_1(0)} \tag{10}$$

It clearly shows that our computations possess the highest grade of trustworthiness. The calculated spectrum of the extinction coefficient $k(\omega)$ for the TiIrBi compound are given in Fig. 8(c). It can be observed in Fig. 8(a) and (c) that $k(\omega)$ and $\varepsilon_2(\omega)$ exhibit similar changes with the increase in photon energy values. Similar to the spectrum of $\varepsilon_2(\omega)$, the threshold value of the extinction coefficient is almost 0.90 eV. As can be seen from these two spectrums, there is a rapid decline after reaching the highest value.

Optical conductivity $\sigma(\omega)$ is one of the prominent optical parameters indicating the carrying of electrons in the current state of electromagnetic radiation. This parameter obtained for a substance puts forward its effectuality in applications of optoelectronic devices and systems. The optical conductivity $\sigma(\omega)$ as a function of photon energy for TiIrBi using mBJ-GGA functional has been calculated and plotted in Fig. 8(d). The optical conductivity begins at approximately 0.90 eV for this compound. It can be seen that the line form of $\sigma(\omega)$ is practically similar to $k(\omega)$ and $\varepsilon_2(\omega)$ spectrums. The highest peak values of $\sigma(\omega)$ for TiIrBi take place in the energy range between 2.2 eV and 7 eV, indicating the visible and ultraviolet regions of the electromagnetic spectrum.

Reflectivity is an optical variable that manifests the reflection of photons from a specific environment. The spectrum of the optical reflectivity for the TiIrBi compound is illustrated in Fig. 8(e). The value of $R(\omega)$ at the zero frequency ($\omega = 0$) boundary is called the static value

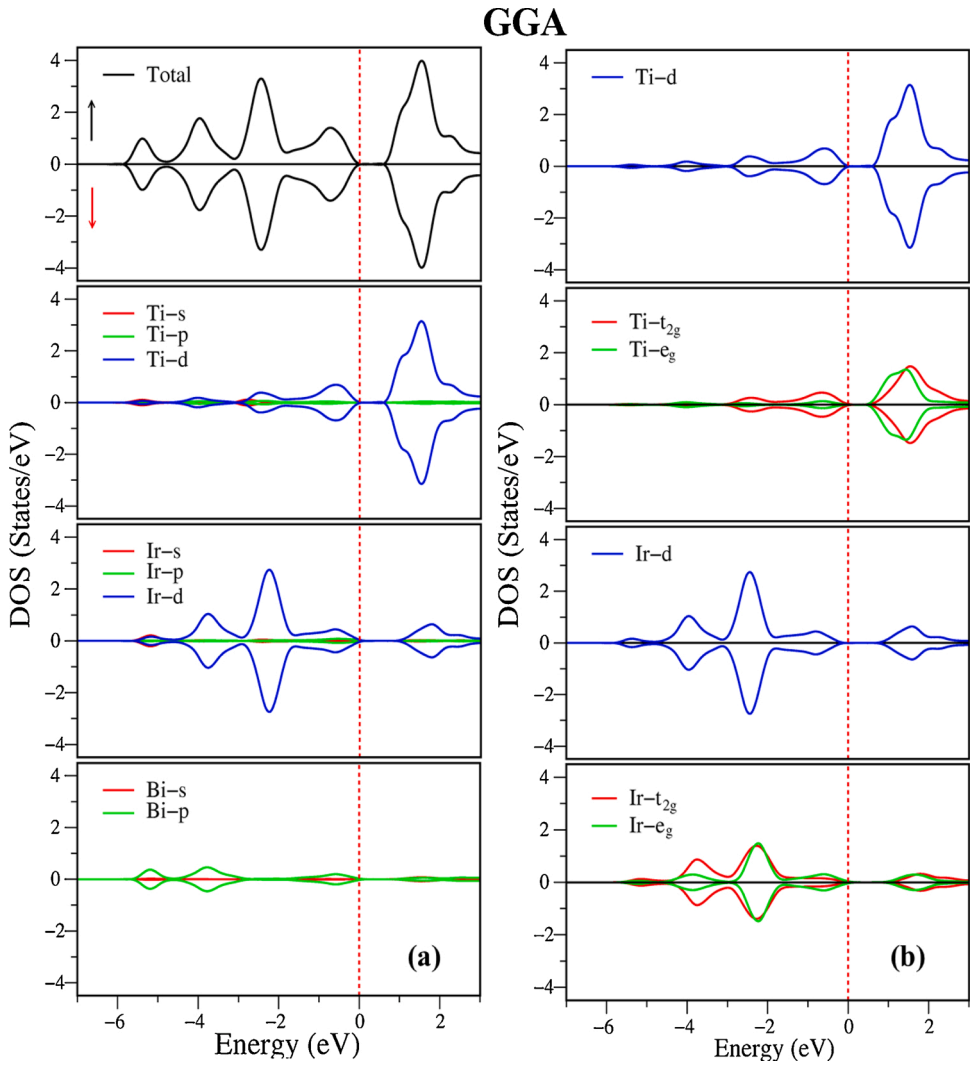

Fig. 5. (a) The spin-polarized total and partial density of electronic states for γ -TiIrBi using GGA, (b) Density of electronic states of t_{2g} and e_g for Ti-*d* and Ir-*d* using GGA.

denoted by *R* (0). The static value of reflectivity is determined as 0.41 for the TiIrBi compound. That is, the reflectivity spectrum begins at 41 % for half-Heusler compound TiIrBi, and after that, the reflectivity attains maximal values about 56 and 55 % for energy values of 2.20 and 3.96 eV, respectively. For this reason, the title compound can act as an armor to shield from high-frequency electromagnetic radiation in the visible and ultraviolet regions of the electromagnetic spectrum in accordance with the high reflectivity grades at these energy values.

3.4. The effect of pressure on the optoelectronic properties

We delved deeper into the electronic and optical characteristics of the TiIrBi compound under pressure from 0 to 50 GPa, with the step of 25 GPa. The computed electronic band structures along the high symmetry directions in the Brillouin zone at these values of the applied pressures are plotted in Fig. 9. At 0 GPa, it is clearly seen that this compound is direct bandgap semiconductors, where the valence band maximum (VBM) and the conduction band minimum (CBM) located at the Γ-point. This direct bandgap value calculated by the GGA-mBJ method is 0.87 eV. However, the analysis of the electronic band structures at 25 GPa and 50 GPa indicates that valence band maximum and conduction band minimum are not at the same symmetry point, which certifies their indirect bandgap nature. These values are found at Γ-point and *X*-point, respectively. As a result, it has become apparent that the TiIrBi compound has a direct bandgap of 0.87 eV without any effect of pressure. However, after applying hydrostatic pressure, its direct bandgap changes into an indirect bandgap of 1.21 eV and 1.26 eV at 25 GPa and 50 GPa, respectively. Similar results have been found in the theoretical study conducted in previous years for half-Heusler compounds. Wei et al. [70] have investigated the electronic structure and optical properties of half-Heusler ZrIrX (X = As, Sb, Bi) compounds under pressure and they reported that the direct bandgap changes to the indirect bandgap with increasing pressure for the ZrIrAs and ZrIrBi compounds.

The variation of the optical properties of half-Heusler materials with pressure is an interesting phenomenon for practical applications. Therefore, the pressure-induced variations of real $\varepsilon_1(\omega)$ and imaginary $\varepsilon_2(\omega)$ dielectric functions in the photon energy range of $0-16$ eV for the TiIrBi compound are calculated using GGA + mBJ approximation and given in Fig. 10(a) and (b), respectively. As can be seen in Fig. 10(a), the calculated values of static dielectric constant $\varepsilon_1(0)$ of the TiIrBi semiconductor are 20.87, 18.02, and 17.20 at 0, 25, and 50 GPa, respectively. Namely, static dielectric constant ($\varepsilon_1(0)$) of this material under changing induced pressure is observed to be decreasing with increasing the pressure. The $\varepsilon_1(\omega)$ spectra are fluctuating to attain their first peak values of 1.76 eV, 1.82 eV, and 2.33 eV at 0 GPa, 25 GPa, and 50 GPa, respectively.

For a deeper understanding of a material's response to the incident

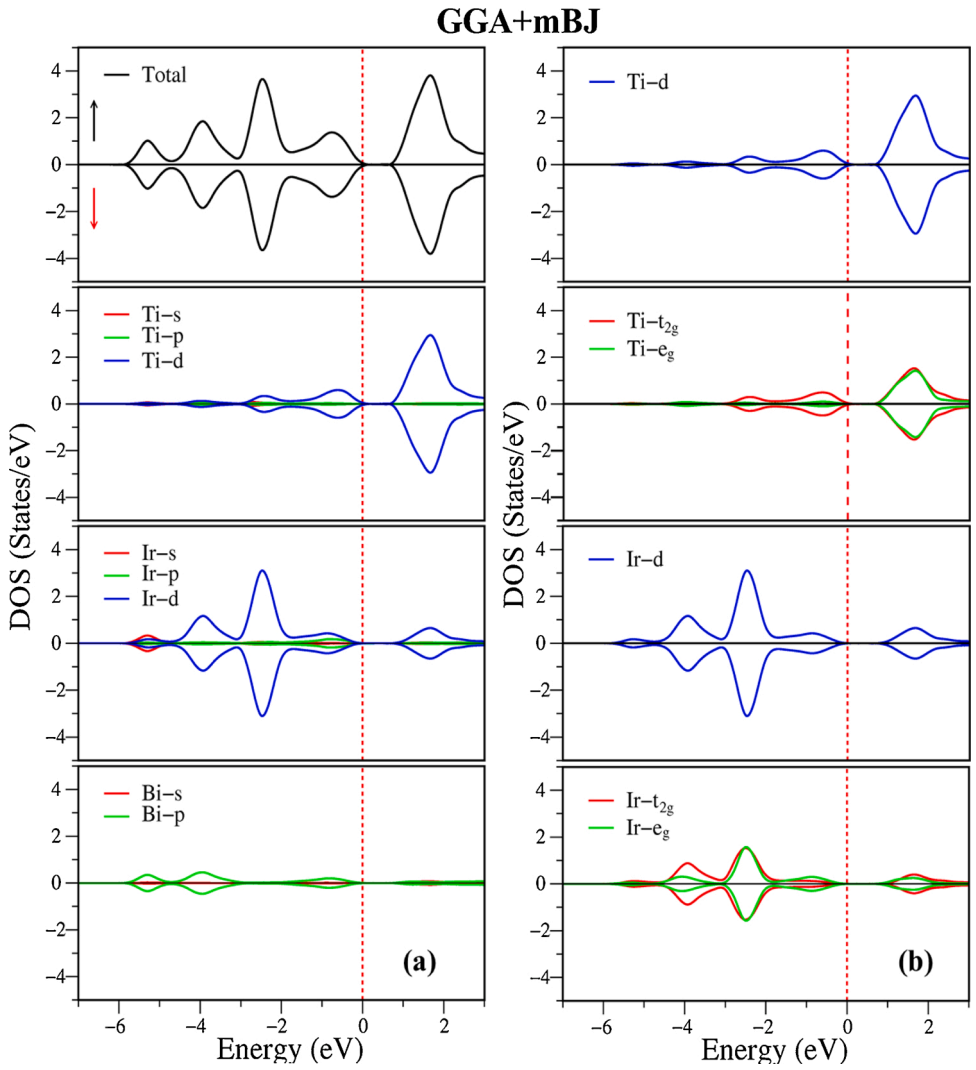

Fig. 6. (a) The spin-polarized total and partial density of electronic states for γ -TiIrBi using GGA + mBJ, (b) Density of electronic states of t_{2g} and e_g for Ti-*d* and Ir-*d* using GGA + mBJ.

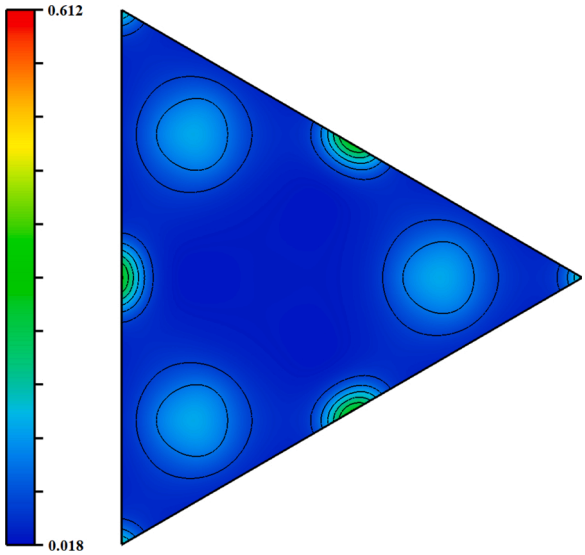

Fig. 7. The charge density plot of the TiIrBi compound along the [111] plane.

photons, imaginary parts of the dielectric function $\varepsilon_2(\omega)$ under various pressures are plotted in Fig. 10(b). It can be clearly observed from Fig. 10(b), the calculated threshold energies in the imaginary parts of the dielectric function using the GGA + mBJ approach are 0.86 eV at 0 GPa, 1.19 eV at 25 GPa, and 1.27 eV at 50 GPa. These values, which are harmonious with the bandgap values obtained from the pressure-dependent electronic band structures of the TiIrBi compound, are in the infrared region in the electromagnetic spectrum. It can be noted from Fig. 10(b) that $\varepsilon_2(\omega)$ increases and approaches to its maximum value 2.20 eV at 0 GPa, 2.73 eV at 25 GPa, and 2.79 eV at 50 GPa. Additionally, the peaks of $\varepsilon_2(\omega)$ spectra minimally shifted toward greater energy values under the effect of pressure.

3.5. *Vibrational properties*

Phonon dispersion curves and detailed phonon state density curves for the γ crystal phase of TiIrBi compound were computed by the PHON program [71], which is based on a supercell approach with the finite displacement technique [72]. Phonon calculations for TiIrBi compound in MgAgAs-type cubic crystal structure with *F-43 m* crystal symmetry were made by setting up a 2 × 2 ×2 supercell containing 96 atoms, and only 0.02 Å displacements of the atoms were allowed. The phonon dispersion curves, total and partial density of states of γ -TiIrBi compound have been plotted in Fig. 11. Besides, the total and partial density

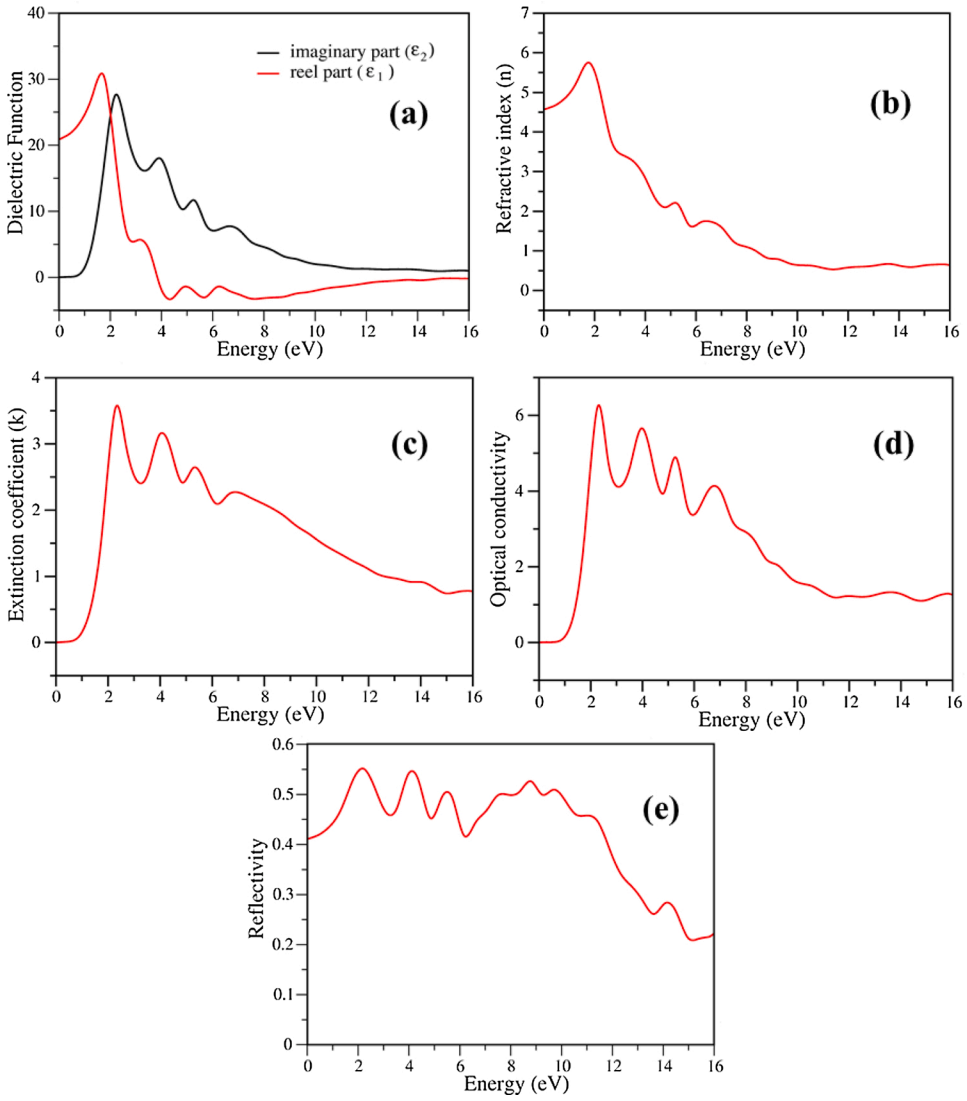

Fig. 8. Optical properties of TiIrBi half-Heusler compound obtained using GGA + mBJ, (a) Real and imaginary part of dielectric function, (b) Refractive index, (c) Extinction coefficient, (d) Optical conductivity, and (e) Reflectivity.

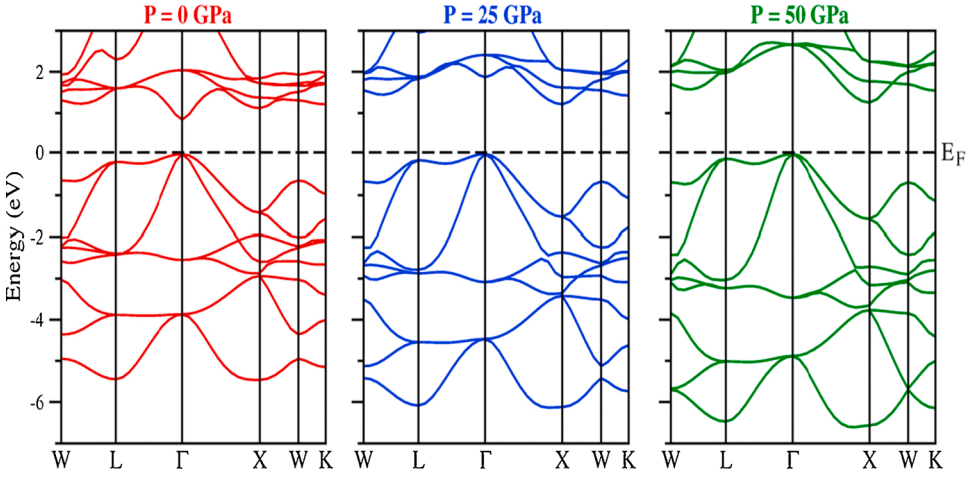

Fig. 9. The electronic band structures of TiIrBi at different pressures (0 GPa, 25 GPa, and 50 GPa).

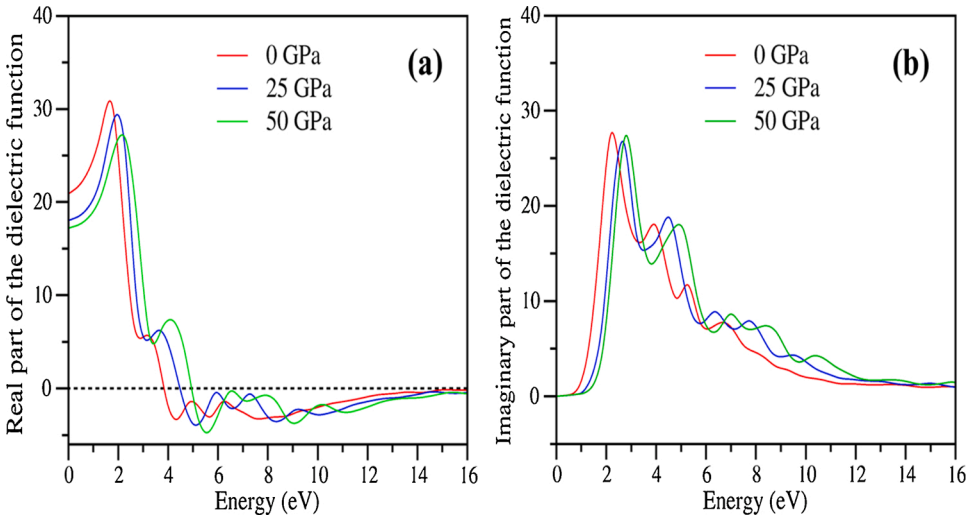

Fig. 10. The pressure dependent (a) real part, and (b) imaginary part of dielectric function of TiIrBi.

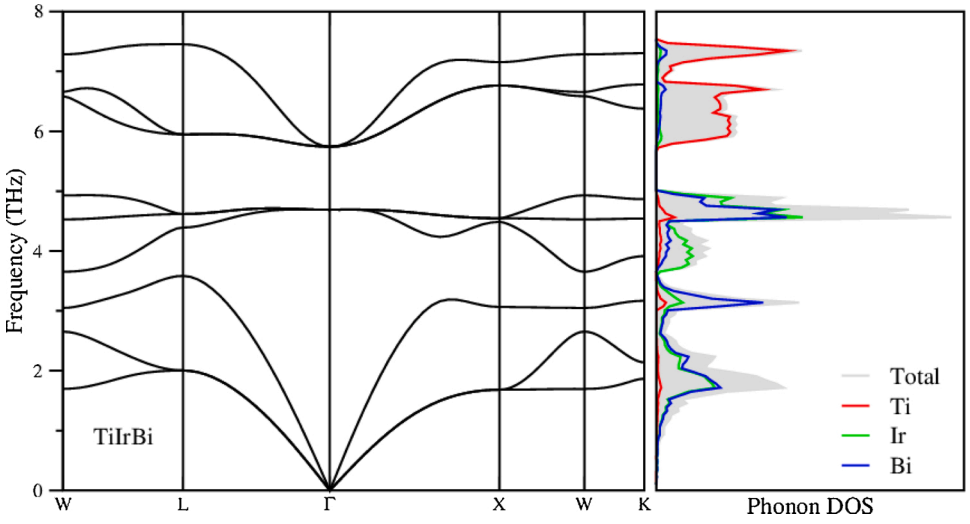

Fig. 11. The phonon dispersion curves, total and partial density of states of γ -TiIrBi compound.

of state curves of this material are shown in detail on the right side of phonon dispersion curves. As can be clearly seen from Fig. 11, there is a total of 9 phonon modes in the phonon dispersion curve of the TiIrBi compound. Three of these phonon modes are acoustic and the rest are optical. It should be emphasized that the TiIrBi compound is dynamically stable in the *F-43 m* type cubic structure because no negative mode is observed in phonon modes. In the phonon dispersion, the total and partial density of state curves given for TiIrBi, there are bandgaps between the acoustic and optical phonon modes as well as the between optical-optical phonon modes. The values of these gaps calculated for this compound are 0.07 THz and 0.81 THz, respectively. Besides, the values of optical phonon modes in the Brillouin zone center are measured as 4.689 THz and 5.742 THz.

As for the total and partial phonon density values, the low energy phonon modes are mainly caused by the vibrations of the Ir and Bi atoms, whereas very small contributions come from the vibration of the Ti atoms. Similarly, the vibrations of the phonon modes between 3.65 THz and 4.93 THz are largely owing to the vibrations of Ir and Bi atoms and the small contributions of Ti atoms. The vibrations of the phonons in high-frequency optical modes (5.74 THz and 7.45 THz) are largely owing to the vibrations of the Ti atoms and small contributions of the vibrations of the Ir and Bi atoms. This situation is expected due to the mass difference between atoms.

4. Conclusions

Self-consistent spin-polarized calculations have been conducted to inquire into the structural stability, electronic, magnetic, optic, and lattice dynamic properties of half-Heusler TiIrBi compound with the 18-valence electron in the cubic MgAgAs-type. Among the structural phases (α, β, and γ), the γ phase has found to be the most stable phase based on both formation enthalpies and energy-volume addictions. When the energy-volume curves plotted for the TiIrBi compound in antiferromagnetic (AFM), paramagnetic (PM), and ferromagnetic (FM) configurations are compared, the paramagnetic configuration is found to be energetically more stable than other magnetic configurations. At the equilibrium lattice constants, the electronic band structures obtained by GGA and GGA + mBJ methods signify TiIrBi compound is a semiconducting material with a direct bandgap of 0.56 eV for GGA and 0.87 eV for GGA + mBJ approaches. The presence of bandgaps can be elucidated with possible *d-d* hybridization between the *d*-electrons of Ti and Ir atoms. This compound has dynamically and thermodynamically stable in the γ structure. Finally, the different optical properties like real and imaginary parts of the dielectric function, refractive index,

extinction coefficient, optical conductivity, and reflectivity have been calculated with GGA + mBJ potential. We hope that our study will stimulate experimental work devoted to the synthesis and applications of TiIrBi as it has been proven to be a promising nominee for technological applications in optoelectronics.

CRediT authorship contribution statement

A. Candan: Investigation, Data curation, Methodology, Formal analysis, Writing - original draft, Writing - review & editing. **A.K. Kushwaha:** Conceptualization, Investigation, Writing - original draft.

Declaration of Competing Interest

The authors declare that they have no known competing financial interests or personal relationships that could have appeared to influence the work reported in this paper.

References

[1] F. Heusler, Uber magnetische manganlegierungen, Verhadl. Deut. Physik. Ges. 5 (1903) 219–223.
[2] R.A. De Groot, F.M. Mueller, P.G. Van Engen, K.H.J. Buschow, New class of materials: half-metallic ferromagnets, Phys. Rev. Lett. 50 (1983) 2024.
[3] D. Kieven, R. Klenk, S. Naghavi, C. Felser, T. Gruhn, I-II-V half-Heusler compounds for optoelectronics: ab initio calculations, Phys. Rev. B 81 (2010), 075208.
[4] S. Ouardi, G.H. Fecher, B. Balke, X. Kozina, G. Stryganyuk, C. Felser, S. Lowitzer, D. Ködderitzsch, H. Ebert, E. Ikenaga, Electronic transport properties of electron- and hole-doped semiconducting $C1_b$ Heusler compounds: $NiTi_{1-x}M_xSn$ (M= Sc, V), Phys. Rev. B 82 (2010), 085108.
[5] S. Kammerer, A. Thomas, A. Hutten, G. Reiss, Co_2MnSi Heusler alloy as magnetic electrodes in magnetic tunnel junctions, Appl. Phys. Lett. 85 (2004) 79–81.
[6] A. Candan, G. Uğur, Z. Charifi, H. Baaziz, M.R. Ellialtıoğlu, Electronic structure and vibrational properties in cobalt-based full-Heusler compounds: a first principle study of Co_2MnX (X= Si, Ge, Al, Ga), J. Alloys Compd. 560 (2013) 215–222.
[7] F. Casper, T. Graf, S. Chadov, B. Balke, C. Felser, Half-Heusler compounds: novel materials for energy and spintronic applications, Semicond. Sci. Technol. 27 (2012), 063001.
[8] S. Berri, First-principles study on half-metallic properties of the CoMnCrSb quaternary Heusler compound, J. Supercond. Nov. Magn. 29 (2016) 1309–1315.
[9] S. Berri, Electronic structure and half-metallicity of the new Heusler alloys PtZrTiAl, PdZrTiAl and $Pt_{0.5}Pd_{0.5}$ ZrTiAl, Chin. J. Phys. 55 (2017) 195–202.
[10] S. Berri, First-principles calculations to investigate the structural, electronic, and half-metallic properties of $Ti_2RhSn_{1-x}Si_x$, $Ti_2RhSn_{1-x}Ge_x$, and $Ti_2RhGe_{1-x}Si_x$ (x= 0, 0.25, 0.5, 0.75, and 1) quaternary Heusler alloys, J. Supercond. Nov. Magn. 32 (2019) 2219–2228.
[11] A. Candan, S. Akbudak, M. Özduran, A. İyigör, An examination of the structural, electronic, elastic, vibrational and thermodynamic properties of Ru_2YGa (Y= Sc, Ti and V) Heusler alloys, Chin. J. Phys. 56 (2018) 1772–1780.
[12] M. Javed, M.A. Sattar, M. Benkraouda, N. Amrane, Structural and mechanical stability, lattice dynamics and electronic structure of the novel CrVZ (Z= S, Se, & Te) half-Heusler alloys, Mater. Today Commun. 25 (2020), 101519.
[13] A. Roy, J.W. Bennett, K.M. Rabe, D. Vanderbilt, Half-Heusler semiconductors as piezoelectrics, Phys. Rev. Lett. 109 (2012), 037602.
[14] D.M. Hoat, M. Naseri, Electronic and thermoelectric properties of RbYSn half-Heusler compound with 8 valence electrons: spin-orbit coupling effect, Chem. Phys. 528 (2020), 110510.
[15] D. Shrivastava, S.P. Sanyal, Theoretical study of structural, electronic, phonon and thermoelectric properties of KScX (X= Sn and Pb) and KYX (X= Si and Ge) half-Heusler compounds with 8 valence electrons count, J. Alloys Compd. 784 (2019) 319–329.
[16] J. Tobola, J. Pierre, S. Kaprzyk, R.V. Skolozdra, M.A. Kouacou, Crossover from semiconductor to magnetic metal in semi-Heusler phases as a function of valence electron concentration, J. Phys. Condens. Matter 10 (1998) 1013.
[17] J. Kangsabanik, A. Alam, Bismuth based half-Heusler alloys with giant thermoelectric figures of merit, J. Mater. Chem. A 5 (2017) 6131–6139.
[18] A. Dey, R. Sharma, S.A. Dar, An extensive investigation of structural, electronic, thermoelectric and optical properties of bi-based half-Heusler alloys by first principles calculations, Mater. Today Commun. 25 (2020), 101647.
[19] O.E. Osafile, J.O. Umukoro, Quasi-harmonic approximation of lattice dynamics and thermodynamic properties of half Heusler ScXSb (x= Ni, Pd, Pt) from first principles, J. Phys. Condens. Matter 32 (2020), 475504.
[20] T. Block, M.J. Carey, B.A. Gurney, O. Jepsen, Band-structure calculations of the half-metallic ferromagnetism and structural stability of full-and half-Heusler phases, Phys. Rev. B 70 (2004), 205114.
[21] F.F. Tafti, T. Fujii, A. Juneau-Fecteau, S.R. de Cotret, N. Doiron-Leyraud, A. Asamitsu, L. Taillefer, Superconductivity in the noncentrosymmetric half-Heusler compound LuPtBi: a candidate for topological superconductivity, Phys. Rev. B 87 (2013), 184504.
[22] Y.J. Zhang, Z.H. Liu, G.D. Liu, X.Q. Ma, Half-metallic fully compensated ferrimagnetism in C1b-type half Heusler compounds $Mn_2Si_{1-x}Ge_x$, J. Magn. Magn. Mater. 387 (2015) 67–71.
[23] G.H. Yu, Y.L. Xu, Z.H. Liu, H.M. Qiu, Z.Y. Zhu, X.P. Huang, L.Q. Pan, Recent progress in Heusler-type magnetic shape memory alloys, Rare Met. 34 (2015) 527–539.
[24] K. Kaur, R. Kumar, D.P. Rai, A promising thermoelectric response of HfRhSb half Heusler compound at high temperature: a first principle study, J. Alloys Compd. 763 (2018) 1018–1023.
[25] W. Al-Sawai, H. Lin, R.S. Markiewicz, L.A. Wray, Y. Xia, S.-Y. Xu, M.Z. Hasan, A. Bansil, Topological electronic structure in half-Heusler topological insulators, Phys. Rev. B 82 (2010), 125208.
[26] C.Y. Guo, F. Wu, Z.Z. Wu, M. Smidman, C. Cao, A. Bostwick, C. Jozwiak, E. Rotenberg, Y. Liu, F. Steglich, H.Q. Yuan, Evidence for Weyl fermions in a canonical heavy-fermion semimetal YbPtBi, Nat. Commun. 9 (2018) 4622.
[27] G. Surucu, A. Candan, A. Erkisi, A. Gencer, H.H. Gullu, First principles study on the structural, electronic, mechanical and lattice dynamical properties of XRhSb (X = Ti and Zr) paramagnet half-Heusler antimonides, Mater. Res. Express 6 (2019), 106315.
[28] G. Surucu, M. Isik, A. Candan, X. Wang, H.H. Gullu, Investigation of structural, electronic, magnetic and lattice dynamical properties for XCoBi (X: Ti, Zr, Hf) Half-Heusler compounds, Phys. B Condens. Matter 587 (2020), 412146.
[29] A. Abada, N. Marbouh, Study of new d° half-metallic half-heusler alloy MgCaB: first-principles calculations, J. Supercond. Nov. Magn. 33 (2020) 889–899.
[30] A. Erkisi, G. Surucu, R. Ellialtioglu, The investigation of electronic, mechanical and lattice dynamical properties of PdCoX (X = Si and Ge) half-Heusler metallics in α, β and γ structural phases: an ab initio study, Philos. Mag. 97 (2017) 2237–2254.
[31] A. Erkisi, G. Surucu, The investigation of electronic, magnetic, mechanical, and lattice dynamical properties of PdMX (M = Cr, Fe and X = Si and Ge) ferromagnetic half-Heusler metallics: an ab initio study, Mater. Res. Express 4 (2017), 066504.
[32] J. Ma, V.I. Hegde, K. Munira, Y. Xie, S. Keshavarz, D.T. Mildebrath, C. Wolverton, A.W. Ghosh, W. Butler, Computational investigation of half-Heusler compounds for spintronics applications, Phys. Rev. B 95 (2017), 024411.
[33] F. Yan, X. Zhang, Y.G. Yu, L. Yu, A. Nagaraja, T.O. Mason, A. Zunger, Design and discovery of a novel half-Heusler transparent hole conductor made of all-metallic heavy elements, Nat. Commun. 6 (2015) 7308.
[34] K. Berland, N. Shulumba, O. Hellman, C. Persson, O.M. Løvvik, Thermoelectric transport trends in group 4 half-Heusler alloys, J. Appl. Phys. 126 (2019), 145102.
[35] T. Sekimoto, K. Kurosaki, H. Muta, S. Yamanaka, Thermoelectric properties of (Ti, Zr,Hf)CoSb type half-Heusler compounds, Mater. Trans. 46 (2005) 1481–1484.
[36] D. Zhao, M. Zuo, L. Bo, Y. Wang, Synthesis and thermoelectric properties of Pd-Doped ZrCoBi half-heusler compounds, Materials 11 (2018) 728.
[37] H. Ma, C.L. Yang, M.S. Wang, X.G. Ma, Y.G. Yi, Effect of M elements (M = Ti, Zr, and Hf) on thermoelectric performance of the half-Heusler compounds MCoBi, J. Phys. D Appl. Phys. 52 (2019), 255501.
[38] R. Gautier, X. Zhang, L. Hu, L. Yu, Y. Lin, T.O.L. Sunde, D. Chon, K.R. Poepplmeier, A. Zunger, Prediction and accelerated laboratory discovery of previously unknown 18-electron ABX compounds, Nat. Chem. 7 (2015) 308–316.
[39] Y. Benallou, K. Amara, B. Doumi, O. Arbouche, M. Zemouli, B. Bekki, A. Mokaddem, Structural stability, electronic structure, and novel transport properties with high thermoelectric performances of ZrIrX (X=As, Bi, and Sb), J. Comput. Electron. 16 (2017) 1–11.
[40] M. Yazdani-Kachoei, S. Jalali-Asadabadi, Topological analysis of electron density in half-Heusler ZrXBi (X= Co, Rh) compounds: a density functional theory study accompanied by Bader's quantum theory of atoms in molecules, J. Alloys Compd. 828 (2020), 154287.
[41] M.K. Bamgbose, Electronic structure and thermoelectric properties of HfRhZ (Z= As, Sb and Bi) half-Heusler compounds, Appl. Phys. A 126 (2020) 1–8.
[42] S. Chibani, O. Arbouche, K. Amara, M. Zemouli, Y. Benallou, Y. Azzaz, B. Belgoumène, M. Elkeurti, M. Ameri, A computational study of the optoelectronic and thermoelectric properties of HfIrX (X= As, Sb and Bi) in the cubic LiAlSi-type structure, J. Comput. Electron. 16 (2017) 765–775.
[43] N. Arikan, G.D. Yildiz, Y.G. Yildiz, A. Iyigör, Electronic, elastic, vibrational, and thermodynamic properties of HfIrX (X= As, Sb and Bi) compounds: insights from DFT-based computer simulation, J. Electron. Mater. 49 (2020) 3052.
[44] W. Huang, X. Wang, X. Chen, W. Lu, L. Damewood, C.Y. Fong, Structural and electronic properties of half-Heusler alloys PtXBi (with X=Mn, Fe, Co and Ni) calculated from first principles, J. Magn. Magn. Mater. 377 (2015) 252–258.
[45] M.I. Babalola, B.E. Iyorzor, A search for half metallicity in half Heusler alloys, J. Magn. Magn. Mater. 491 (2019), 165560.
[46] S. Ouardi, C. Shekhar, G.H. Fecher, X. Kozina, G. Stryganyuk, C. Felser, S. Ueda, K. Kobayashi, Electronic structure of Pt based topological Heusler compounds with $C1_b$ structure and "zero band gap", Appl. Phys. Lett. 98 (2011), 211901.
[47] C. Mondal, C.K. Barman, S. Kumar, A. Alam, B. Pathak, Emergence of topological insulator and nodal line semi-metal states in XX′Bi (X= Na, K, Rb, Cs; X′= ca, Sr), Sci. Rep. 9 (2019) 527.
[48] L. Mikaeilzadeh, A. Tavana, F. Khoeini, Electronic structure of the PrNiBi half-Heusler system based on the σ GGA+ U method, Sci. Rep. 9 (2019) 20075.
[49] G. Kresse, J. Furthmüller, Efficiency of ab-initio total energy calculations for metals and semiconductors using a plane-wave basis set, Comput. Mater. Sci. 6 (1996) 15–50.
[50] G. Kresse, J. Furthmüller, Efficient iterative schemes for ab initio total-energy calculations using a plane-wave basis set, Phys. Rev. B 54 (1996) 11169.
[51] P.E. Blöchl, Projector augmented-wave method, Phys. Rev. B 50 (1994) 17953.
[52] J.P. Perdew, K. Burke, M. Ernzerhof, Generalized gradient approximation made simple, Phys. Rev. Lett. 77 (1996) 3865.

[53] A.D. Becke, E.R. Johnson, A simple effective potential for exchange, J. Chem. Phys. 124 (2006), 221101.
[54] F. Tran, P. Blaha, Accurate band gaps of semiconductors and insulators with a semilocal exchange-correlation potential, Phys. Rev. Lett. 102 (2009), 226401.
[55] D. Koller, F. Tran, P. Blaha, Merits and limits of the modified Becke-Johnson exchange potential, Phys. Rev. B 83 (2011), 195134.
[56] H.J. Monkhorst, J.D. Pack, Special points for Brillouin-zone integrations, Phys. Rev. B 13 (1976) 5188.
[57] M. Methfessel, A.T. Paxton, High-precision sampling for Brillouin-zone integration in metals, Phys. Rev. B 40 (1989) 3616.
[58] K. Momma, F. Izumi, VESTA 3 for three-dimensional visualization of crystal, volumetric and morphology data, J. Appl. Crystallogr. 44 (2011) 1272–1276.
[59] F. Murnaghan, The compressibility of media under extreme pressures, Proc. Natl. Acad. Sci. 30 (1944) 244.
[60] E. Zhao, Z. Wu, Electronic and mechanical properties of 5d transition metal mononitrides via first principles, J. Solid State Chem. 181 (2008) 2814.
[61] J. Camargo-Martínez, R. Baquero, Performance of the modified Becke-Johnson potential for semiconductors, Phys. Rev. B 86 (2012), 195106.
[62] S. Chibani, O. Arbouche, M. Zemouli, K. Amara, Y. Benallou, Y. Azzaz, B. Belgoumène, A. Bentayeb, M. Ameri, Ab initio prediction of the structural, electronic, elastic, and thermoelectric properties of half-Heusler ternary compounds TiIrX (X= As and Sb), J. Electron. Mater. 47 (2018) 196–204.
[63] M.M. Obeid, M.M. Shukur, S.J. Edrees, R. Khenata, M.A. Ghebouli, S.A. Khandy, A. Bouhemadou, H.R. Jappor, X. Wang, Electronic band structure, thermodynamics and optical characteristics of $BeO_{1-x}A_x$ (A = S, Se, Te) alloys: insights from ab initio study, Chem. Phys. 526 (2019), 110414.
[64] B. Bencherif, A. Abdiche, R. Moussa, R. Khenata, X. Wang, Pressure effect on structural, electronic optical and thermodynamic properties of cubic $Al_xIn_{1-x}P$: a first-principles study, Mol. Phys. 118 (2020), e1608380.
[65] L. Azzouz, M. Halit, A. Allal, S. Maabed, M. Bouchenafa, R. Ahmed, T. Seddik, A. Bouhemadou, R. Khenata, Structural, electronic, optical and elastic properties of layered rhombohedral compounds $ALaSe_2$ (A=K, Rb): insights from an ab initio study, Int. J. Mod. Phys. B 33 (2019), 1950084.
[66] G. Marius, The Physics of Semiconductors: Kramers-kronig Relations, Springer, Berlin Heidelberg, 2010, pp. 775–776.
[67] S. Azam, S.A. Khan, R. Khenata, S.H. Naqib, A. Abdiche, Ş. Uğur, A. Bouhemadou, X. Wang, An ab-initio investigation of the electronic structure, chemical bonding and optical properties of Ba_2HgS_5 semiconductor, Mol. Phys. 118 (2020), e1587026.
[68] M. Irfan, M.A. Kamran, S. Azam, M.W. Iqbal, T. Alharbi, A. Majid, S.B. Omran, R. Khenata, A. Bouhemadou, X. Wang, Electronic structure and optical properties of TaNO: an ab initio study, J. Mol. Graph. Model. 92 (2019) 296–302.
[69] N. Yaqoob, G. Murtaza, M.W. Iqbal, N.A. Noor, A. Mahmood, S.M. Ramay, N.Y. Al-Garadi, Study of half metallic nature and transport properties of $XMnSe_2$ (X= Ca, Sr and Ba) compounds via ab-initio calculations, J. Mater. Res. Technol. 9 (2020) 10511–10519.
[70] J. Wei, G. Wang, Electronic structure, optical and thermoelectric properties of half-Heusler ZrIrX (X = As, Sb, Bi): a first principles study, J. Comput. Electron. 16 (2017) 535–541.
[71] D. Alfè, PHON: a program to calculate phonons using the small displacement method, Comput. Phys. Commun. 180 (2009) 2622–2633.
[72] K. Parlinski, Z.Q. Li, Y. Kawazoe, First-principles determination of the soft mode in cubic ZrO_2, Phys. Rev. Lett. 78 (1997) 4063.